Elastic wave simulation for buffer rod tapering

by

T.S. Oud

to obtain the degree of Bachelor of Science
at the Delft University of Technology,
to be defended publicly on Thursday July 17, 2017 at 11:00 AM.

Student number:	4381343	
Project duration:	April 24, 2017 – August 17, 2017	
Thesis committee:	S. Mastromarino,	TU Delft, supervisor
	Dr.ir. M. Rohde,	TU Delft
	Prof.dr.ir. J. L. Kloosterman,	TU Delft

An electronic version of this thesis is available at http://repository.tudelft.nl/.

TU Delft

Nomenclature

ϵ	Strain [-]
λ	First Lame parameter [Pa]
μ	Second Lame parameter [Pa]
ω	Angular frequency [s^{-1}]
ϕ	Scalar wave potential [m]
ψ	Vector wave potential [m]
Θ	Angle [°]
A	Area [m^2]
C	Elasticity matrix [Pa]
c	Speed of elastic wave [$m * s^{-1}$]
F	Force [N]
f	Frequency [s^{-1}]
K	Bulk modulus [Pa]
l	Length [m]
n	Direction vector [-]
P	Pressure [Pa]
R	Reflection coefficient [-]
T	Stress [Pa]
t	Time [s]
u	Displacement/Elongation [m]

Abstract

With the development of molten salt reactors, it arises the necessity of accurate measurements of fuel properties. Conventional measuring techniques for viscosity can not be used due to high fuel temperature and radioactivity. A new viscometer is being developed based on ultrasonic techniques. By guiding ultrasonic waves formed by a transducer through a buffer rod into the liquid fuel and measuring the reflected waves, the attenuation, linked to viscosity, can be determined. This buffer rod ensures the effectiveness of the piezo-electric material in the transducer. Modern piezo-electric elements become depolarized at the temperature of these fuels.

Mode conversion of ultrasonic waves at the rod boundaries result in trailing echoes inside the buffer rod. This leads to low signal to noise ratio in the viscosity measurement. Tapering of buffer rods will lead to an increase in signal to noise ratio. Using COMSOL Multiphysics, multiple tapered rods with different angles have been simulated. It was found that for a certain buffer rod geometry, an optimal angle exists. After increasing this angle, the trailing echoes will not be suppressed anymore.

Simulating ultrasonic waves in buffer rods with accurate wave velocities for shear and longitudinal waves requires a mesh constant higher than 13 elements per wavelength. A simulation like this will have a velocity error lower than 1%. These kinds of high accuracy simulations are not done within this research.

Realistic buffer rod design simulations using COMSOL need to be done on a machine with sufficient hard disk space available. Simulations with accurate wave velocities require a large amount of memory and very long computation time. The COMSOL model, made in this research, is able to determine an optimal angle for a future buffer rod.

Other options to reduce trailing echoes, like cladding and different rod materials, are also promising and need to be investigated in future research.

Contents

1

Introduction

The increase in energy requirement caused by an increase in world population combined with global warming problems lead to the need for a clean and sustainable energy source. Currently, the necessity of energy is satisfied mainly using fossil fuels. Although this type of energy is cheap and immediate, it accelerates climate change. For this reason, it is necessary to focus on alternative sustainable energy sources. New nuclear reactor designs look promising as a solution to this problem. The reactor design treated in this research is the Molten Salt Fast Reactor(MSFR), which is one of the generation IV reactors. The generation IV reactors will excel in areas of sustainability, safety and economic feasibility. These were proposed in the year 2000.

1.1. SAMOFAR

The research conducted in this project is part of the SAMOFAR project. Safety Assessment of the Molten Salt Fast Reactor is a European project that will prove the innovative safety concepts of a molten salt reactor using experiments and computer simulations. Another purpose is to acquire stakeholders for future development of the MSFR.

1.2. Molten salt reactor

The most remarkable aspect of this generation IV reactor is that the fuel is in liquid form. Thus, the fuel simultaneously contains the fissile material and is also a transport medium for the heat. A great advantage, of these new generation reactors concerning security is the fact that it is not possible to have a meltdown due to the liquid nature of the fuel. Moreover, the molten salt fuel also has a low pressure due to its high boiling point and low vapor pressure which will significantly reduce the risk of reactor vessel breakage or fuel leakage.

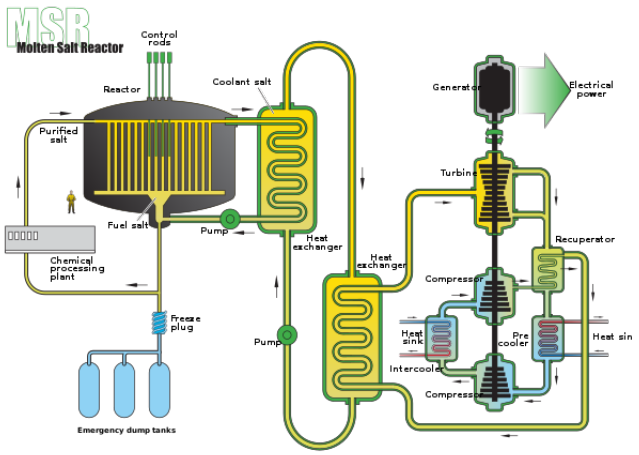

Figure 1.1: Figure of Molten Salt Fast Reactor [1]

Regarding the sustainability of these reactors, MSRs can operate in a breeding cycle with Uranium-238. The amount of this isotope is 99.3% of all natural Uranium available on Earth. Light-water reactors use mainly U-235, which is much rarer. Moreover MSR's can use Thorium as fertile matter in a breeding cycle, of which there is approximately three times as much as Uranium. MSR's can also work with nuclear waste produced by Light-water reactors. This reduces the nuclear waste storage problem. All these innovative features, make the MSR a very promising solution to the global energy problem.

1.3. Viscosity measurement

A part of the SAMOFAR research is the determination of thermodynamic properties of the fuel salt such as viscosity and density. This is needed to understand the fluid behavior in the reactor circuit. Conventional measuring methods can not be used due to the high temperature of the salt and it's radioactivity. Measuring viscosity therefore requires an innovative technique with ultrasonic sound waves produced by transducers. However the temperature where modern piezo-electric transducers become depolarized is exceeded by the fuel temperature. So in this way the transducer can not send and detect ultrasonic pulses [2]. With the use of a buffer rod to dissipate the heat, ultrasonic waves from a transducer are guided to the salt and reflected back and measured by the transducer. In the amplitude difference compared to the original wave, information can be found regarding the viscosity. This amplitude difference depends on a relation between the viscosity and the attenuation of the wave.

1.4. Experimental set up

In order to design a new viscosity measurement technique, it is necessary that experiments are done. A ultrasonic transducer is connected to a waveform generator and to an oscilloscope to measure the returning waves. The transducer is positioned on top of a copper rod as can be seen in figure 1.2.

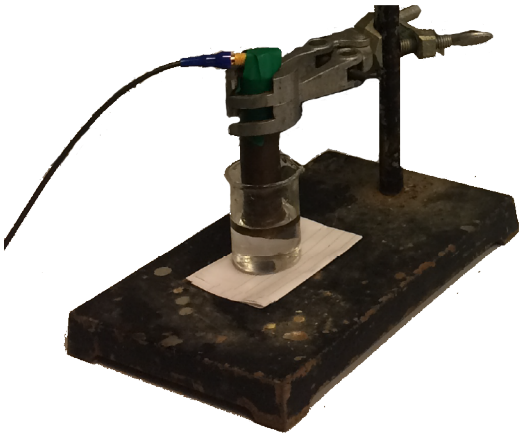

Figure 1.2: Figure of experimental setup [7]

A layer of glycerin between the transducer and the buffer rod is used to mitigate the high acoustic impedance difference between air and the copper rod.

1.5. Research goals

The use of a buffer rod comes with a problem. When the ultrasonic waves travel through the rod, mode conversion from longitudinal to transversal waves takes place at the boundaries of the rod. These reflected shear waves travel with a fraction of the speed of the original longitudinal wave. When the shear wave meets a boundary, mode conversion results in the generation of another wave front that is delayed by a certain time determined by the speed of the shear waves and the rod geometry. It is the presence of these so called trailing echoes that cause a distortion in the viscosity measurement. The goal of this research is to investigate if the trailing echoes can be minimized by tapering of the rod with a certain angle using computer models with finite element methods. The program used to do this is COMSOL Multiphysics [4]. To determine this, first the model has to be verified by comparing simulations with experimental results. When this is done, the model can be used to determine optimal rod tapering at a certain rod length. In the end it is desirable that for a given rod geometry, an optimal tapering angle can be determined.

This report starts with a thorough theoretical explanation of elastic waves. After that, all details of the COMSOL model are discussed followed by results acquired from these models. Finally a conclusion is made.

2

Theory

Sound waves in solids are called elastic waves and depend on the elastic properties of the material in which they propagate. Therefore, it is necessary to give a description of elasticity in solids to describe acoustic waves. Subsequently elastic waves will be discussed for the one and three dimensional case. This includes a thorough mathematical model of the waves. Next the phenomenon of mode conversion is explained and finally the formation of trailing echoes is treated.

2.1. Theory of elasticity

2.1.1. Stress tensor

Waves manifest itself in solids through displacement and simultaneously through pressure changes in time. In continuum mechanics, strain and stress are expressed in tensors. A force acting on a solid will cause a deformation to the shape. These deformations can be parallel to the force which is hydrostatic or perpendicular which is a shear strain or stress. Stress can be written as follows.

$$T = n \cdot \sigma \tag{2.1}$$

where

$$\sigma = \begin{bmatrix} \sigma_{11} & \sigma_{12} & \sigma_{13} \\ \sigma_{21} & \sigma_{22} & \sigma_{23} \\ \sigma_{31} & \sigma_{32} & \sigma_{33} \end{bmatrix} \tag{2.2}$$

The diagonal terms are longitudinal stresses and the off diagonal terms are shear stresses. n is the direction vector of the stress.

2.1.2. Strain tensor

If the strain is small enough it can be described by the linearized strain tensor below [12]:

$$\epsilon = \frac{1}{2}[\nabla u + (\nabla u)^T] \tag{2.3}$$

where u is the displacement vector. This expression for strain is only valid when $|\frac{\partial u}{\partial x}| \ll 1$. With the use of Hooke's law, which states that stress is a linear function of strain, one can write the stress as follows with elasticity matrix C.

$$T = C\epsilon(u) \tag{2.4}$$

In the two dimensional case, this can be written as below using the first and second Lamé parameters:

$$T(u) = \lambda(\nabla \cdot u) + 2\mu\epsilon(u) \tag{2.5}$$

where λ is the first Lamé parameter and μ is the shear modulus. This relation will be used later to derive the solution of the wave equations for longitudinal and shear waves. Thus, the strain tensor can be used to write the stress tensor in a convenient way using Hooke's law.

2.2. Elastic waves in solids

In this section, two fundamentally different kinds of waves will be treated, which are very important for this research. These are longitudinal and shear waves. In a liquid medium, transversal waves can not be sustained because shear stress will simply result in a flow. Shear waves can only exist at very high frequencies in a fluid for a limited amount of time. However in solids the particles do not flow, therefore shear waves are present and will propagate and have a large impact on the behavior of the waves. A description of shear waves is crucial to fully describe elastic wave phenomena in solids. The purpose of this section will be to determine the wave equation in a solid medium for both shear and longitudinal waves.

2.2.1. One-dimensional

First, a 1D model of solids is considered. A 1D object with length l is elongated by a displacement ∂u due to a force F on a surface A which creates a stress $T = \frac{F}{A}$. This will lead to a net stress of $\partial T = l(\frac{\partial T}{\partial x})$.The strain in one dimension can be written as follows [3].

$$\epsilon = \frac{\partial u}{l} = \frac{\partial u}{\partial x} \tag{2.6}$$

Where l is the length of the 1D model in this case.

Newton's law states the following:

$$\frac{\partial T}{\partial x} = \rho \ddot{u} \tag{2.7}$$

where ρ is the density. This says that the equation of motion includes only the pressure gradient. In combination with Hooke's law this will result in the next expression,

$$\frac{\partial^2 u}{\partial x^2} = \frac{\rho}{c}\frac{\partial^2 u}{\partial t^2} \tag{2.8}$$

which is the wave equation in a 1D solid where c is the specific speed of the waves. Solving the differential equation gives the following solutions [3].

$$u = Ae^{j(\omega t - \beta x)} + Be^{j(\omega t + \beta x)} \tag{2.9}$$

These are the well known solutions for the wave equation where $\beta = \frac{\omega}{V_L}$ is the wave number with a wave velocity of

$$V_L = \sqrt{\frac{c}{\rho}}. \tag{2.10}$$

and the frequency ω. c here is the elasticity matrix for one dimension.

2.2.2. Full solution

Equation number 2.7 and Hooke's law $T(u) = C\epsilon(u)$ combined will give the wave equation as is displayed below. C here is a fourth order tensor with the elastic properties of the material. For the derivation of shear and longitudinal waves later it is easier to pick

$$\rho\frac{\partial^2 u_i}{\partial t^2} = \frac{\partial}{\partial x_i}[(a-2b)\frac{\partial u_i}{\partial x_i}] + b\frac{\partial^2 u_i}{\partial x_j^2} + b\frac{\partial}{\partial x_i}(\frac{\partial u_i}{\partial x_j}) \tag{2.11}$$

This notation uses two spatial variables x_i and x_j.

$$\rho\frac{\partial^2 u_i}{\partial t^2} = (a-b)\frac{\partial^2 u_i}{\partial x_i^2} + b\frac{\partial}{\partial x_i}(\frac{\partial u_i}{\partial x_j}) \tag{2.12}$$

Where $a = \lambda + 2\mu$ $b = \mu$. These quantities are often called C_{11} and C_{44} in the literature. These are also part of the fourth order stress tensor with elastic properties. Expanding to three dimensions the equation can be expressed in vectorial form.

$$\rho\frac{\partial^2 u_i}{\partial t^2} = (a-b)\vec{\nabla}(\vec{\nabla}\cdot\vec{u}) + b\nabla^2\vec{u} \tag{2.13}$$

After this, it is convenient to use that any vector can be expressed as the gradient of a scalar potential and the cross product of a vector potential. This creates two new concepts: the scalar potential ϕ and the vector potential $\vec{\psi}$. With these new potentials the displacements can be written as follows.

$$\vec{u} = \vec{\nabla}\phi + \vec{\nabla} \times \vec{\psi} \tag{2.14}$$

When using this expression in the equation of motion, it is useful to use the following vector identities. These identities combined with a mathematical trick that is done after this, will result in a relatively simple deduction of longitudinal and shear wave velocities.

$$\vec{\nabla} \times (\vec{\nabla}\phi) \equiv 0 \tag{2.15}$$

This is for the scalar potential. For the vectorial potential the following holds.

$$\vec{\nabla} \cdot (\vec{\nabla} \times \vec{\psi}) \equiv 0 \tag{2.16}$$

Stating the curl free component and the divergence free component and using the identities above result in:

$$\vec{\nabla}(\rho\frac{\partial^2\phi}{\partial t^2} - a\nabla^2\phi) + \vec{\nabla} \times (\rho\frac{\partial^2\vec{\psi}}{\partial t^2} - b\nabla^2\vec{\psi}) = 0 \tag{2.17}$$

where the first term is scalar and the second a vector, which can only be the case if both terms are zero. This gives the final differential equations which govern longitudinal and shear waves respectfully.

$$\rho\frac{\partial^2\phi}{\partial t^2} = a\nabla^2\phi \tag{2.18}$$

$$\rho\frac{\partial^2\vec{\psi}}{\partial t^2} = b\nabla^2\vec{\psi} \tag{2.19}$$

Because of the choice of a and b, the first term is the equation for longitudinal waves while the second only describes shear waves. Solving these equations gives $V_L = \sqrt{\frac{\lambda+2\mu}{\rho}}$ for longitudinal wave speed and $V_T = \sqrt{\frac{\mu}{\rho}}$ for shear wave speed. Both shear and longitudinal waves are shown in figure 2.1. The shear wave speed is always a fraction of the longitudinal wave speed. This fraction is

$$\frac{V_T}{V_L} = \frac{\sqrt{\frac{\mu}{\rho}}}{\sqrt{\frac{\lambda+2\mu}{\rho}}} = \sqrt{\frac{\mu}{\lambda+2\mu}} \tag{2.20}$$

The properties of shear waves compared to longitudinal waves differ considerably when considering different materials. The ratio given above actually is really important regarding trailing echoes. With copper this ratio is around 0.48 [7].

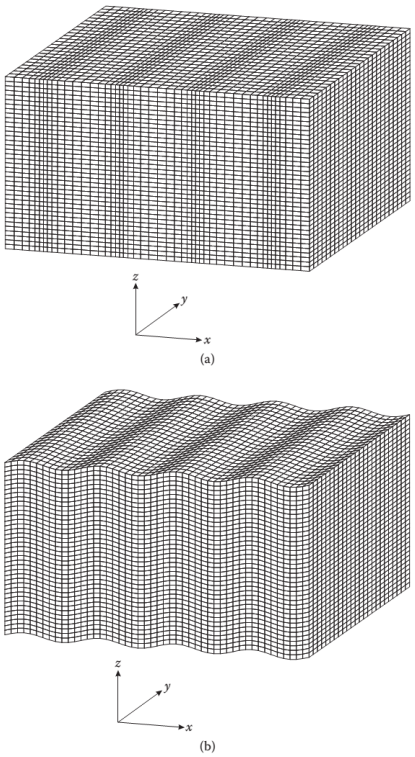

Figure 2.1: Longitudinal (a) vs transversal (b) waves [3]

2.3. Mode conversion

When elastic waves in solids meet a boundary between different media at a certain angle, the energy of the reflected or transmitted wave is converted into two kinds of waves. Shear waves and longitudinal waves. Longitudinal waves can cause vibrations of particles in a transversal mode and also the other way around. In this research only reflection takes place due to the acoustic impedance difference of copper and air. This is proven in the next section. No solid-liquid interface is treated in this research [13].

2.3.1. Transmission and reflection

At boundaries, similar to waves in optics, Snell's law determines how waves behave.

$$\frac{sin(\theta_1)}{sin(\theta_2)} = \frac{V_1}{V_2} \tag{2.21}$$

Equation 2.21 governs the behavior of both reflection and refraction.

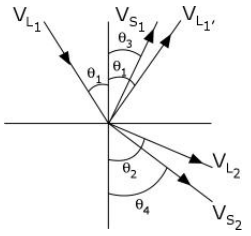

Figure 2.2: Mode conversion at boundary from longitudinal to shear waves [13]

In the figure above, mode conversion from longitudinal to shear is shown for transmission and reflection. Naturally, this is also possible from shear to longitudinal. However in this case only reflection is relevant. Considering the acoustic impedances of the rod material and

air, one can calculate the amount of transmission from the rod to air. This depends on the acoustic impedance difference of the two media. Calculating this for a copper air interface results in a reflection of nearly 100% because acoustic impedance of copper is way larger than for air. The acoustic impedance is defined as follows [10]

$$Z \equiv \frac{p}{v} \tag{2.22}$$

where p is pressure and v is the speed of the particles. This impedance is analogous with the impedance in an electric circuit. The reflection coefficient between two media will therefore be:

$$R = \frac{Z_2 - Z_1}{Z_1 + Z_2}. \tag{2.23}$$

During reflection of elastic waves, part of the wave is converted to a longitudinal wave and another part to a transversal wave. The ratio between the two is determined by Snell's law and is given below for different occasions. For conversion from shear to shear and from shear to Longitudinal respectively the reflection coefficients are the following [3].

$$R_{SS} = -\frac{sin(2\Theta_s)sin(2\Theta_l) - \frac{V_L^2}{V_S^2}cos^2(2\Theta_s)}{(2\Theta_s)cos(2\Theta_l) + \frac{V_L^2}{V_S^2}cos^2(2\Theta_s)} \tag{2.24}$$

$$R_{LS} = \frac{2\frac{V_L}{V_S}sin(2\Theta_s)cos(2\Theta_s)}{(2\Theta_s)cos(2\Theta_l) + \frac{V_L^2}{V_S^2}cos^2(2\Theta_s)} \tag{2.25}$$

From longitudinal to shear and from longitudinal to longitudinal mode conversion looks like the equations displayed below.

$$R_{LS} = \frac{2\frac{V_L}{V_S}sin(2\Theta_l)cos(2\Theta_s)}{(2\Theta_s)cos(2\Theta_l) + \frac{V_L^2}{V_S^2}cos^2(2\Theta_s)} \tag{2.26}$$

$$R_{LL} = \frac{sin(2\Theta_s)sin(2\Theta_l) - \frac{V_L^2}{V_S^2}cos^2(2\Theta_s)}{(2\Theta_s)cos(2\Theta_l) + \frac{V_L^2}{V_S^2}cos^2(2\Theta_s)} \tag{2.27}$$

In the above equations Θ_l corresponds to the longitudinal wave and Θ_S to the shear. The same applies to V_l and V_s.

2.3.2. Material properties

The behavior of shear and longitudinal waves highly depends on the elastic properties of the material. Due to difference in wave speed between shear and longitudinal, shear waves are reflected under a smaller angle with the normal due to Snell's law. The angles under which the shear waves are reflected depends on the speed of these waves. Thus shear wave forming is governed by the elastic properties of the material. Specifically in this case the first and second Lamé parameters as is shown in section 2.2.2 and also the density are the relevant properties.

2.4. Trailing echoes

After mode conversion has taken place twice, once from longitudinal to shear and subsequently from shear to longitudinal, a second pulse or trailing echo is acquired. There will be several different trailing echoes due to forming of shear waves from longitudinal waves with different incoming angles with the boundary, however one of them will dominate. This is because shear wave forming is optimal for specific materials under a specific angle as is shown in [7].

Minimizing these trailing echoes can be done in a number of ways. In this research only tapering of the buffer rod is investigated. In several investigations it has been shown experimentally that tapering significantly reduces trailing echoes [14] [9]. Regarding an optimal angle, it is assumed that for different geometries different angles with the least trailing echoes will exist.

With an increase in angle of incidence for longitudinal waves comes a reduction in shear wave forming after a certain angle.

Cladding a layer of a certain material to the rod with a specific acoustic impedance can also limit mode conversion. The acoustic impedance must be such that mode converted waves are transmitted instead of reflected.

Research of different materials with different elastic properties and thus different elastic wave velocities will also be necessary to optimize trailing echo reduction.

3

Computational Method

All simulations in this research are done with COMSOL Multiphysics [4]. Specifically the solid mechanics module of COMSOL. In the following chapter the two dimensional model using Cartesian and cylindrical coordinate system will be discussed. The purpose of these models is to confirm the results acquired by experiments and also to investigate the influence of tapering. The ultimate goal is to determine an optimal angle for the reduction of trailing echoes. Finally it is desirable to simulate a double tapered rod to validate measurements.

3.1. General model properties

The following sections explain carefully all the steps required to make the COMSOL models that are being used in this research.

3.1.1. Definitions

Each COMSOL model begins with the possibility to assign definitions or parameters. This includes the pulse that is applied to the boundary of the rod which will be explained in the physics section. A sine multiplied by a Gaussian is used as a pulse which can be see in figure 3.1.

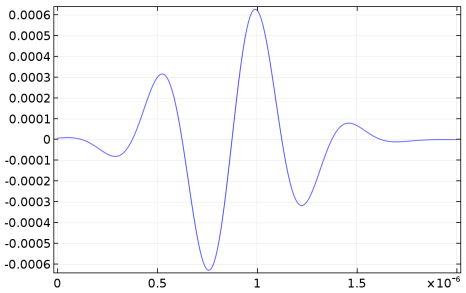

Figure 3.1: In this figure the displacement pulse used in the model is shown. The vertical axis is displacement [m] and the horizontal axis is time [s].

The frequency of the pulse used in the simulations is 2 MHz. In the experiments a frequency of 3.5 MHz is used, but this requires significantly more computation time and memory. The amplitude of the pulse will have to change when different rod lengths are modeled. For the estimation of the amplitude the following equation is used.

$$K = -V\frac{dP}{dV} \tag{3.1}$$

where K is the bulk modulus of the material, P is the pressure and V is the volume. This

equation can be written in another way using $V = A\Delta l$.

$$K = -Al\frac{\Delta P}{A\Delta l} = -l\frac{\Delta P}{\Delta l} \tag{3.2}$$

Δl can be interpreted as the amplitude of the pulse and $\frac{\Delta l}{l}$is the amplitude relative to the length of the rod. This relation predicts that an increase in rod length requires also an increase in pulse amplitude to maintain useful results. This only gives an indication on what the displacement of elastic waves will be due to a certain transducer pressure.

3.1.2. Geometry

The rods have a cylindrical shape, therefore in a two dimensional Cartesian model the geometry will simply be a rectangle. For the model with the cylindrical coordinate system a axi symmetric two dimensional component is used in COMSOL. In both cases the dimensions of the copper rods are determined by rods used in the experiments.

3.1.3. Material

The material used in the simulations is copper. This is specified in the materials node in COMSOL. All the properties from the material are taken from this materials node. However it is not necessary to select a material since all elastic properties can also be mentioned in the physics part of the program that will be discussed later. Different rod materials can be easily simulated using this model, by simply entering the elastic properties of the desired material into the model.

3.1.4. Study type

A time dependent study is used to visualize the behavior of the wave. Although a time step size can be specified, the final step size used in the solution is determined by the COMSOL solver. Also a time range needs to be specified. In this research the time range is set such that the wave travels twice back and forth in the rod. All solvers used in the simulations are the default COMSOL solvers.

3.2. Physics

For all COMSOL models of the rod, the physics interface Solid Mechanics is used, which is part of the structural mechanics module of COMSOL [5]. This module automatically creates a node which specifies a linear elastic material. In the axial symmetry model, COMSOL also accounts for the symmetry. subsequently, the pressure waves need to be specified. This is where the pulse mentioned above is used. To produce a pressure wave, the boundary condition prescribed displacement is used. Prescribed displacement creates the pulse as a function of time and can be set to vibrate in a certain direction. In this model, the vibration direction is the Z direction only. So the pressure wave is defined in COMSOL as a longitudinal displacement wave. Instead of prescribed displacement, boundary load can also be used. This will apply a pressure to the boundary instead of a displacement. All the other boundary conditions on the rod are set to free. The free boundary condition implies that the outside of the rod is a vacuum with zero stress in all directions. This is acceptable because acoustic impedance difference between air and copper is large enough as is explained in the chapter 2.

Equations in COMSOL

Each boundary and domain condition has an equation in COMSOL. The equations in the linear elastic material node are the following.

$$\rho\frac{\partial^2 u}{\partial t^2} = \nabla \cdot S + F_V \tag{3.3}$$

Where S equals Stress. In chapter 2 stress was called T. F_V is a force dependent on starting conditions in the model. The elastic deformation equation is given in equation 3.4.

$$\epsilon = \frac{1}{2}[(\nabla u)^T + \nabla u] \tag{3.4}$$

This is also the strain tensor from the previous chapter. The free boundary condition is automatically assigned in this model. This basically means there are no pressures or constraints acting on the boundaries which have the free condition.

Next the equation for the displacement at the transducer location is shown.

$$u = u_{0,z} \tag{3.5}$$

where the second term is equal to the time dependent pulse which is displayed in section 3.1.1.

3.3. Discretization

3.3.1. Mesh

In order to get an accurate result, the mesh has to be accordingly. In a simple 2D model, which does not take into account the cylindrical symmetry, the mesh criteria can be formulated as follows. Since it is a elastic wave model, a certain amount of mesh elements per wavelength are required for accurate simulation. This results in criteria that are similar to Nyquist's limit which says in this case that there should be at least two mesh elements per wavelength to build an accurate model. In sampling, a sample frequency that is lower than twice the frequency that is measured will give aliasing. With the modeling of ultrasonic waves this will cause the presence of wrong solutions. However, in the modeling of ultrasonic waves, this value must be higher. Previous bachelor research [7] found that this number should be 8 for a square mesh. This is also the case in this research [8] only here a free triangular mesh is used. The wavelength that is used here should be from the shear waves because they have the smallest wavelength. This mesh is the same for the r and z direction in the cylindrical model and also for the x and y direction in the Cartesian model. In this research triangular and quadrilateral mesh elements are used. COMSOL has algorithms for determining a free triangular mesh. Within this mesh a maximum element size can be assigned. Because a rectangular area can not be filled by equally shaped triangles, COMSOL uses an algorithm to fill up the space as efficiently as possible. For the quadrilateral mesh the mapped function is used with a certain mesh density in the r and z direction. This results in a discretization which uses square elements. Mesh optimization for both discretization types is necessary and is discussed in the results chapter.

3.3.2. Courant-Friedrichs-Lewy number (CFL)

In time dependent computer models, time is also discretized. Specifically for waves, this discretization is related to the spatial mesh size. This relation is given by the CFL number. The CFL number is defined as follows for longitudinal waves [6].

$$CFL = \frac{\Delta t c_L}{\Delta L} \tag{3.6}$$

where ΔL is maximum element size and Δt is the time step in the model which corresponds to a certain CFL number. It needs to be noted here that solvers in COMSOL pick a CFL number dependent on convergence of the model. The time step assigned to the model only influences the first step in the time dependent simulation. After that the solver algorithm which is used takes over.

A Phd research [6] on this subject done with mesh constants from 6 to 30 elements per wavelength has shown that for different CFL numbers wave speed errors decrease with increasing mesh constants. With a CFL of 0.2, which is used in this research, wave velocity error is reduced to around 1% after a mesh constant of 12 per wavelength.

3.4. Tapered rod

In this section, several tapered rod simulations will be discussed.

3.4.1. Single tapered

The modeling of a rod with a slight angle brings more challenges because now there is a part where square mesh elements can not be used due to the angle. In the model of this research a mesh is used which is the same as previous mesh for the straight part and a free triangular mesh with a maximum element size as is previously discussed. Also a mesh was used which used coarser elements at the start of the rod. This was essentially just a mapped mesh using quadrilateral elements which were no longer perfect squares. However this produced wrong solutions where the second trailing echo has a larger amplitude than the first for small angles. Therefore this method can not be used. All models of single tapered rods in this research are 83 mm long and have a width of 20 mm.

3.4.2. Double tapered

In the experiments, a double tapered rod is used. This shape is used because of heat dissipation and practicality in a final set up to measure the viscosity of the salt. Therefore this shape must also be modeled. The mesh for this model is essentially the same as for the single tapered rod, except now there are two tapered parts. This obviously increases computation time. The rod which is used in measurements is 30 cm long and has a tapering angle of 1.15 degrees.

4

Results

This chapter starts with the optimization of the mesh for the straight rod model. Secondly, displacement plots are shown for this model. Subsequently the transducer measurements in the model are displayed for the tapered models. These results give an optimal angle. Finally the double tapered rod is discussed which is made in order to validate experimental measurements [10].

4.1. Straight rod

The first step in this research was to make a model of a straight copper rod which takes into account the cylindrical symmetry. This model calculates everything in 2D but also corrects for the actual 3D geometry. In COMSOL this is called a 2D axi symmetric model.

4.1.1. Mesh optimization

In all computational models done with finite element methods optimization of the mesh is imperative. While this is less important to visualize the waves, the optimization becomes relevant to produce solutions that are physically valid. It is expected that after a certain amount of mesh elements per wavelength the solution will be constant. To investigate this, a quantity that highly depends on mesh size is chosen and compared with solutions with different mesh sizes. This quantity is then plotted versus mesh size to obtain a graph. The quantity chosen in this particular case is the total displacement u at the axis of the cylinder squared and multiplied by the Z coordinate in the cylindrical coordinate system. This quantity is then integrated over Z to acquire a single value that can be plotted versus mesh size per wavelength.

$$Q = \int_0^Z u^2 Z dZ \tag{4.1}$$

The previous integral is calculated at time $1.92e^{-5}s$. This value should converge to a certain number when mesh size is increased. The mesh number where this quantity stops changing will be the best possible mesh for this model. This is done for a rod of length 83 mm and width 20 mm at a frequency of 2 MHz. Here only the quadrilateral mesh is used. Increasing the mesh size up to 16 mesh elements per wavelength, the displacement was still not converging. From these results it can be concluded that this method is too sensitive to changes in mesh size.

Another way to measure mesh adequacy, is to calculate the longitudinal wave speed error for different mesh numbers per wavelength. Wave speed is both an important physical parameter and a value that should converge to a constant when increasing the mesh. This is done in the figure below for triangular and quadrilateral meshes.

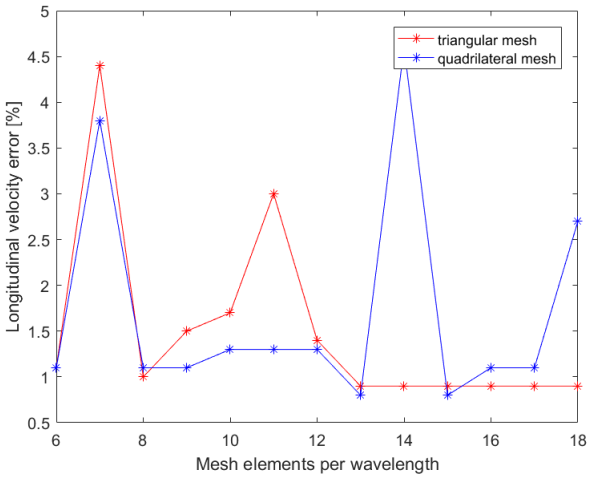

Figure 4.1: Figure of the mesh optimization [11]. The number of mesh elements per wavelength is plotted against the longitudinal wave velocity error. For quadrilateral discretization, no convergence was found. Wave velocity error is below 1% for a mesh with 13 elements per wavelength.

From this it can be concluded that triangular mesh elements provide a reliable error after a mesh constant of 13 elements per wave length. Unfortunately the quadrilateral mesh is not converging within the given mesh constants. Another thing that needs to be mentioned is that triangular mesh simulations take longer and also occupy twice the memory of simulations using quadrilateral elements. This will be a significant problem when running simulations of large rods on a regular laptop. The conclusion from this is that more memory and time is required for realistic simulations.

4.1.2. 2D Displacement plots

To visualize the waves, displacements plots are made in COMSOL. These show the total amount of displacement in all directions. Within the solid mechanics physics branch, also total pressure or stress can be plotted. However these quantities did not visualize the elastic waves in a way that both longitudinal and shear waves are clearly visible. Later these quantities are used in a way to create transducer like measurements in the simulation. The following results are made with a 16 mesh elements per wavelength simulation using a free triangular spatial discretization and a CFL number of 0.2. The plots are created by revolving the solution, which only consists of half of the rod width due to symmetry, around the Z axis. Then a section of this solution looks like a 2D displacement plot while in fact the solution is 3D. COMSOL always simulates different dimensional models with 3D properties.

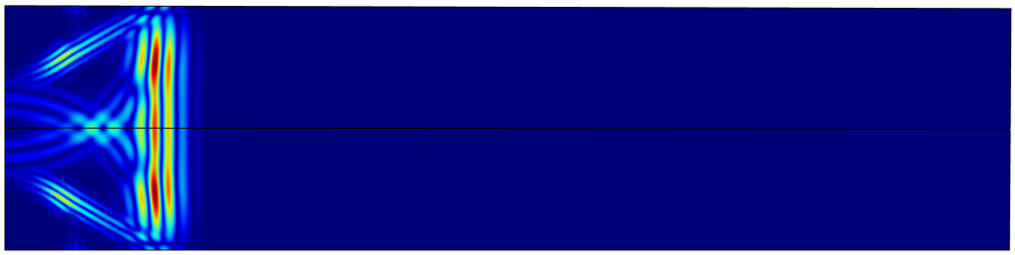

Figure 4.2: Displacement plot at time $3.6e^{-6}s$. The wave is generated at the left side of the rod. This is also where the transducer is positioned in experiments. The difference in wavelength between longitudinal waves and shear waves can be noticed. The color red represents maximum amplitude and dark blue is zero amplitude.

In figure 4.2 it is clearly visible that reflected longitudinal waves from the beginning of the pulse interfere with the last part of the pulse. This interference can be reduced with a pulse with a higher frequency. A larger rod geometry, which means a longer travel path for the reflected longitudinal waves, will also minimize this interference.

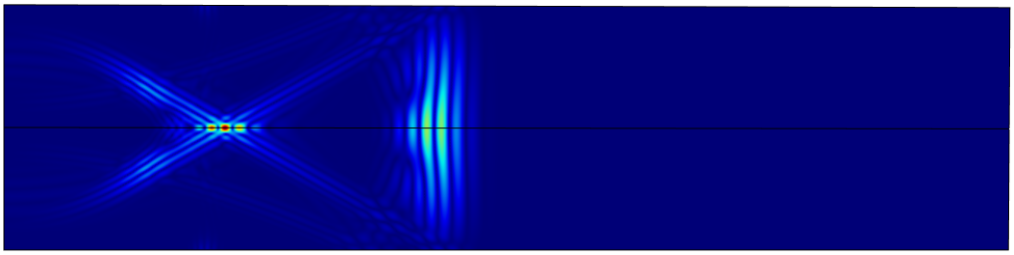

Figure 4.3: Displacement plot at time $8.64e^{-6}s$. Shear waves result in a X pattern. This the same model as in figure 4.2, only at a later time point.

In figure 4.3, the forming of shear waves due to mode conversion at the boundaries of the rod is clearly visible. It is shown by H. Froeling [7] that these are in fact shear waves. This can also be understood by observing the change in wavelength compared to the original pulse. Furthermore the X pattern that is formed by shear waves is clearly visible here. This pattern is also shown in a simulation made by Ihara et al. [9].

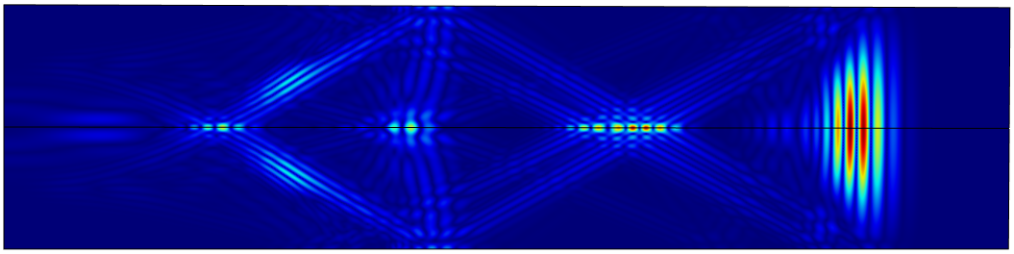

Figure 4.4: Displacement plot at time $1.62e^{-5}s$. At this point in time, the second wavefront, which is the first trailing echo, can be seen. When comparing the wave at the right of the image with the original wave in figure 4.2, one notices the dispersion.

Figure 4.4 displays the formation of a second wave front due to mode conversion from shear to longitudinal waves. This second wave front will be the first trailing echo which will be visualized in the next part using probe plots in COMSOL.

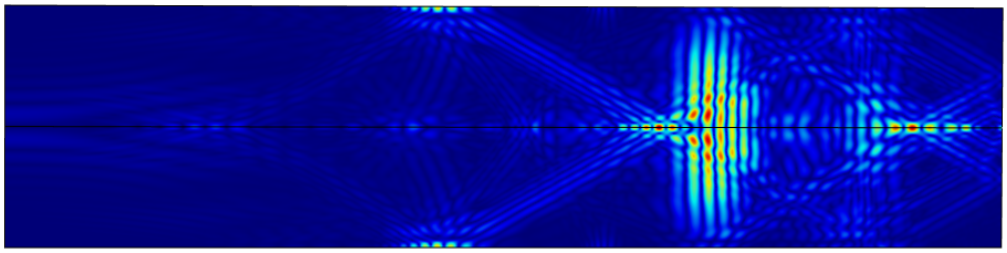

Figure 4.5: Displacement plot at time $2.43e^{-5}s$. In this figure the wave can be seen after reflection at the end of the rod. The visible wave is now propagating to the left. The displacement plot becomes too chaotic to identify each individual wave.

In the last displacement plot the returning wave after reflection with the other side of the rod is displayed. After this reflection, displacement plots become rather chaotic. This makes identifying different waves difficult.

4.1.3. Probe plots

In order to compare the simulations with the experiments, some kind of measurement at the location of the transducer needs to be done. COMSOL has a function called probe which does exactly this. In this case pressure is measured because this is closely related to the voltage which is measured in the experiments. The exact quantity that is used is called the second Piola-Kirchhoff stress in the Z direction. This is in order to replicate the behavior of a ultrasonic transducer which mostly measures longitudinal elastic waves.

4.1.4. Comparison with 2D model

The major difference with the 2D Cartesian ultrasonic waves model [7] is the intensity of shear waves at $r = 0$ at the symmetry axis of the cylinder. This can be explained by the fact that reflected waves will all come together at $r = 0$ which causes the high intensity. These can also be explained as computational singularities that do not influence important physical results.

4.2. Tapered rod

In the tapered simulations a rod of length 83 mm and width 20mm is used with a pulse frequency of 2 MHz. First a simulation with no tapering is done for comparison. The results from this simulation are displayed below in table 4.1.

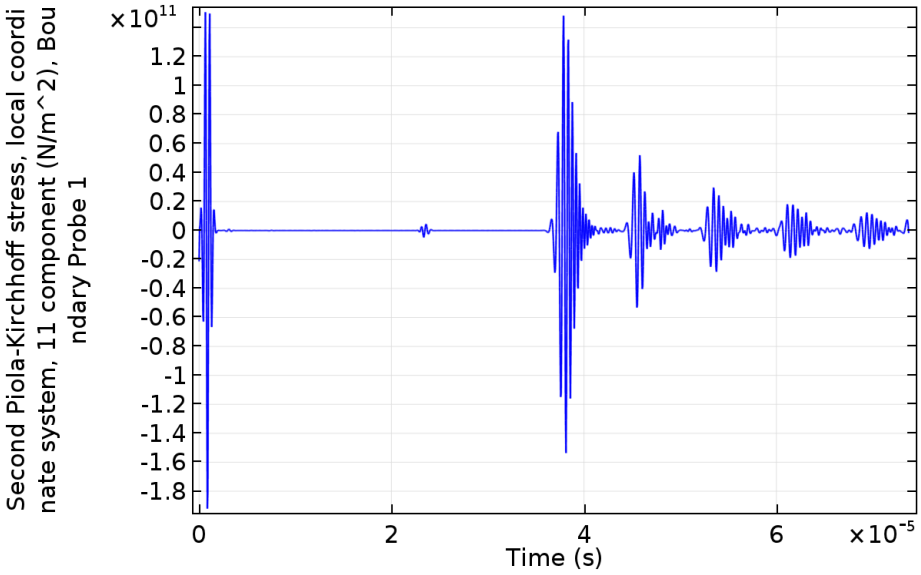

Figure 4.6: In this figure a probe plot of a 0 degree tapered rod is shown. This corresponds to the model in 4.1. This is a measurement at the transducer location. Like the transducer, also pressure is measured here.

Next the simulation with the angle which gives the most trailing echo suppression is shown. This occurred at an angle of 1.25 degrees. The influence of increasing tapering angle is minimal after this angle as can be seen in appendix A.

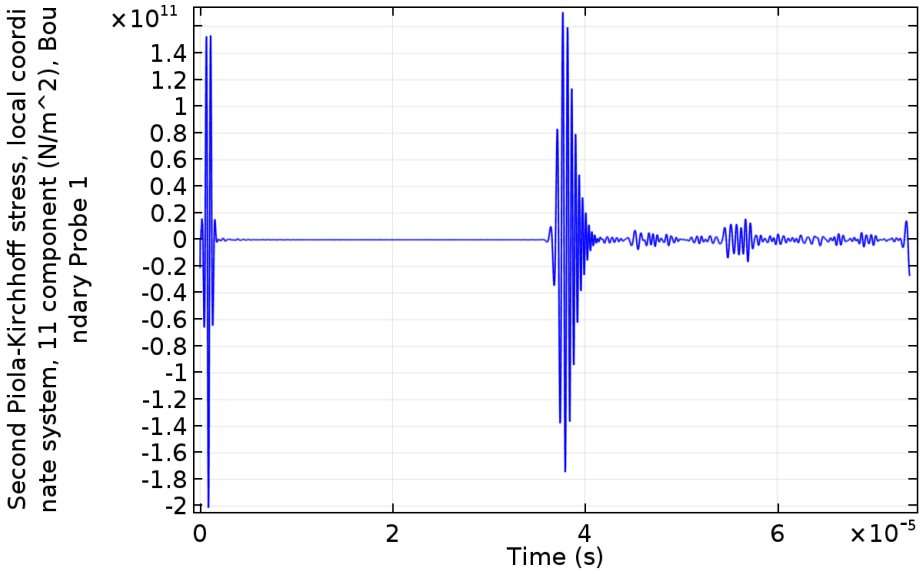

Figure 4.7: In this figure a probe plot of the 1.25 degree tapered rod model is shown. This is the optimal angle for amplitude suppression of the first trailing echo. This is a measurement at the transducer location.

When looking at the ratio between the first trailing echo and the reflection, this gives 0.4 for the 0 degrees tapering and 0.036 for the 1.25 degree tapering simulation. This means tapering can only reduce trailing echoes for around 90% percent according to this simulation. It is important to note that this does only include the first trailing echo. The second trailing echo remains considerably large and only reduces by approximately 50% when comparing to the non tapered model.

What is plotted here is the pressure in the Z direction. An extraordinary result is that after a certain angle the second trailing echo becomes larger than the first. This is also a phenomenon in the measurements that should be further investigated.

The rest of the simulations with different angles are displayed in appendix A. All suppression values of these models are displayed in the following table.

Table 4.1: Trailing echo amplitude suppression for all simulations in %

Tapering angle	1^{st} echo suppression [%]	2^{nd} echo suppression [%]	3^{rd} echo suppression [%]
0	0	0	0
0.25	12	35	7
0.5	68	57	36
0.75	78	39	57
1	80	43	71
1.25	87	43	64
1.5	87	56	71
1.75	87	65	71

4.2.1. Dispersion

In the simulations one can observe that the returning waves are broader than the starting waves. Also the returning pulse consists of several waves with different frequencies. This is due to dispersion which is caused by the different frequencies that are present in the pulse. This is a phenomena that is always present and can not be eliminated fully. Therefore the returning waves will always appear longer than the original wave at the start of wave. This phenomena is also clearly visible in the research of Ghose et al. [8].

The broadening of the pulse is also caused by shear waves that are traveling at different angles and form wavefronts right after each other. These wavefronts will subsequently merge

and appear like a broadened wave. This is also explained in the theory.

4.2.2. Optimal angle

Ihara et al. used a tapering angle of 1.15 degrees. [9]. The straight part of the rod suggested by Ihara is 50 mm and the tapered part is 250 mm long. However all investigations regarding an optimal angle concluded that this can only be determined for specific geometries. This means that the optimal angle for a 20 cm rod is different than the one for a 30 cm rod. Frequency will also have a significant influence to the forming of shear waves. In the case of this research the optimal angle is determined for a 83 mm rod. Because it is possible to determine this angle using this model, it can also be done with other geometries if needed. A 83 mm rod was used to reduce computation time and at the same time allow for enough shear waves to be converted. From these results it can be concluded that for this geometry an optimal angle exists around 1.25 degrees.

4.3. Double tapered rod

Simulations of a 30 cm double tapered rod at limited accuracy, have shown that shear intensity increases at the beginning of the rod. Once the wave passes the middle of the rod, shear intensity drops again which is desirable. However the increase in intensity in the first part of the rod, causes this geometry to be less efficient at reducing trailing echoes when compared to a single tapered rod.

Now the ultimate goal in validating the COMSOL model is to compare the results with the experimental data of the double tapered rod. This is a rod with a length of 30 cm and an angle of 1.15 degrees. However to exactly replicate the experiments one needs to use a frequency of 3.5 MHz which leads to very long computation time. In order to minimize this time, a frequency of 2 MHz is used here. Also the wave velocities of both longitudinal and shear waves must be correct. However this requires a very high mesh constant. All these reasons make validating the experiments with a COMSOL simulation impossible on a regular laptop with limited hard disk space.

4.4. Conclusion

With buffer rods with a length of 83 mm, an optimal angle of 1.25 degrees was determined. All simulations regarding tapering use a mesh constant which causes a maximum error in wave speed of approximately 5%. More accurate wave speeds can be simulated with greatly increasing computation time and hard disk space requirement. This research is done with a regular laptop, which has limited hard drive disk space. This significantly limits the ability to accurately model the longitudinal elastic wave velocity. With a triangular mesh, a mesh constant greater than 13 elements per wavelength is needed for the correct velocity. This does not even include the correct shear wave speed which will most likely require double the value of mesh constant to simulate correctly.

Therefore future research regarding an optimal angle for a certain rod geometry must be done at a high mesh constant to ensure correct wave speeds and thus correct reflection angles during the mode conversion. This means using a machine with adequate hard drive space. Also it must be possible for this machine to run simulations for a long time.

5

Conclusion

In order to achieve accurate simulation data at high frequencies (above 2 MHz) combined with correct wave velocities takes a very long time. Also a large amount of memory is needed. A simulation done with triangular mesh with 16 elements per wave length uses over 40 GB of memory. What is important to note is that mesh optimization is only done for longitudinal waves. Shear waves, which are essential in this research, have a wavelength of approximately half the longitudinal wavelength. This will result in a mesh that is twice as small and will use twice the amount of memory. Therefore simulations can only be done realistically with a frequency of 2 MHz and incorrect wave velocities on a regular laptop. However these results have shown that rod tapering works in reducing trailing echoes. Also optimal angles can be determined regarding trailing echo reduction of the first echo. This is the most important conclusion from this research. Experiments done with ultrasonic transducers can be simulated in COMSOL. But in order to replicate measurements and to give advice on future buffer rod designs, simulations need to be done on more powerful machines. The primary reason for why this is not done in this research is that a lot of time was consumed by the mesh optimization with quadrilateral elements. It was concluded that this kind of mesh is not adequate in this model. A important conclusion is that not all distortion caused by trailing echoes can be eliminated by the tapering of the rod. Moreover, a way for lowering computational time and efficiency should be investigated in future research.

5.1. Discussion

The inability of the quadrilateral mesh to converge to a reliable wave speed error might be due to the fact that element size is incorrectly measured. Here the sides of the square are taken as the size. However the largest part of the square is the diagonal. This changes mesh densities by a factor of $\sqrt{2}$. But this should not influence the longitudinal wave speed.

Also more attention needs to be paid to error estimation in determining optimal tapering angles. Different simulations with smaller angle differences around 1.25 degrees need to be done for a decisive optimal angle.

The COMSOL models for the determination of optimal angles use a mesh which consists of free triangular for the angled parts and mapped quadrilateral for the straight part. This gives a boundary between the two meshes which might influence the solution. For instance the wave velocity might change causing additional delays in the trailing echoes. More accurate models would use only a triangular mesh which eliminates this boundary.

5.2. Recommendation

Because tapering of the rod can not reduce trailing echoes to an acceptably low level, other options must be researched. One promising feature is the adding of a layer around the rod. This layer can be made of a certain material with reflection and transmission properties determined by the impedance which can also reduce trailing echoes. The technique described is called cladding. This can also be modeled in COMSOL together with tapering.

The second issue is simulating what happens at the solid-liquid interface. Verification that suppression of trailing echoes indeed enables viscosity measurements, will be necessary for the design of a buffer rod.

Lastly, looking how temperature distribution and heat dissipation in rod influence elastic material properties at different locations is also important. This will in turn change the behavior of elastic waves. In a final design for buffer rods it has to be taken into account.

A

Results for different angles

Probe plots of pressure at the location of the transducer are displayed for several angles. The decay in trailing echo intensity is clearly visible in these graphs. These are all results from a model with a 83 mm copper rod and a frequency of 2 MHz. Plotted on the vertical axis is the stress in the Z direction which is the Piola-Kirchhoff stress in COMSOL.

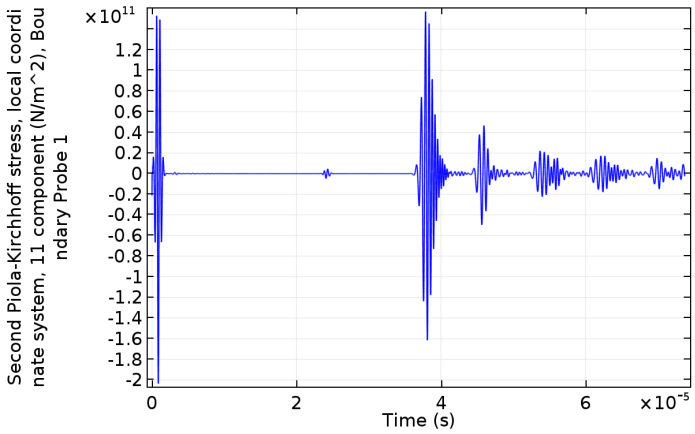

Figure A.1: Probe plot 0.25 degrees tapering

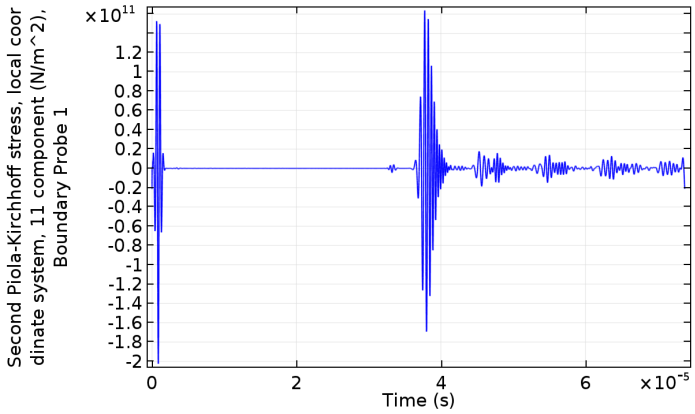

Figure A.2: Probe plot 0.5 degrees tapering. This is a measurement at the transducer location.

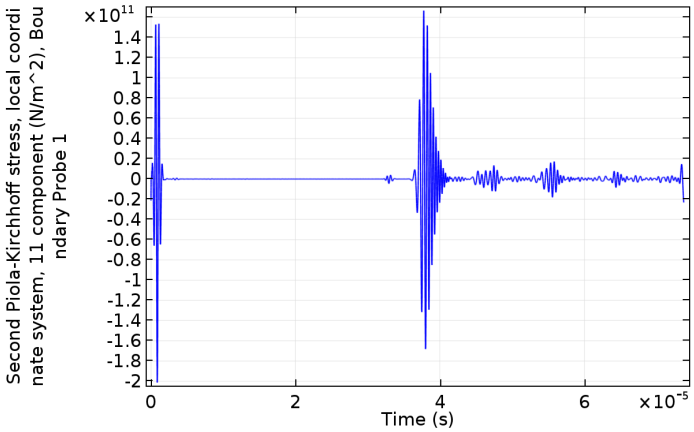

Figure A.3: Probe plot 0.75 degrees tapering. This is a measurement at the transducer location.

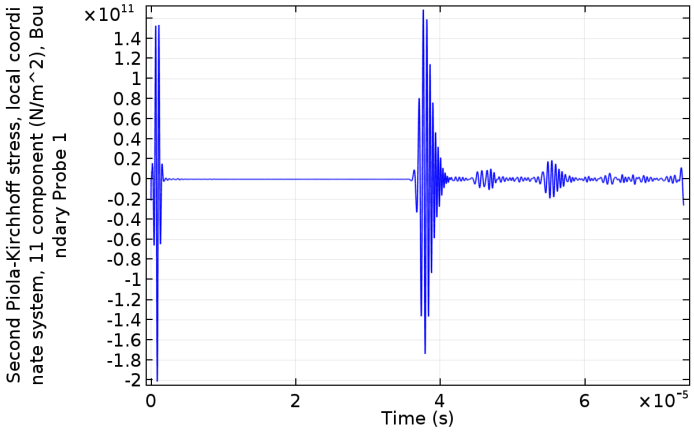

Figure A.4: Probe plot 1 degrees tapering. This is a measurement at the transducer location.

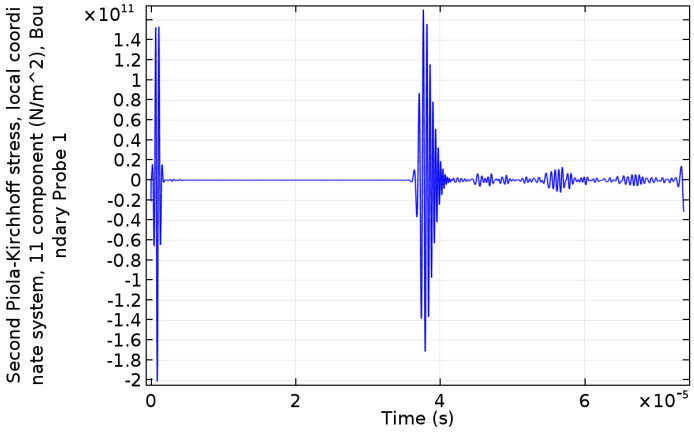

Figure A.5: Probe plot 1.5 degrees tapering. After this angle the first trailing echo can not be more suppressed. This is a measurement at the transducer location.

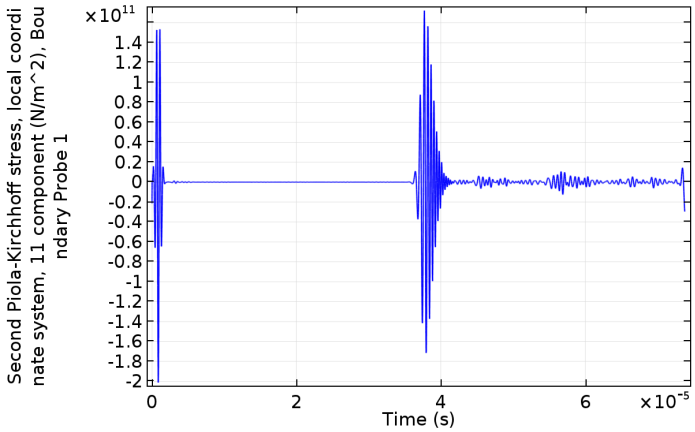

Figure A.6: Probe plot 1.75 degrees tapering. This is a measurement at the transducer location.

Bibliography

[1] Molten salt reactor. URL https://www.gen-4.org/gif/jcms/c_42150/molten-salt-reactor-msr.

[2] F.B. Cegla. *Ultrasonic waveguide sensors for fluid characterisation and remote sensing*. PhD thesis, Imperial College London, 2006.

[3] J.D.N. Cheeke. *Fundamentals and Applications of Ultrasonic Waves*. CRC series in pure and applied physics. CRC Press, 2010.

[4] COMSOL. *version 5.2a*. 2015.

[5] COMSOL. *Structural Mechanics Module*. 2015.

[6] M.B. Drozdz. *Efficient finite element modelling of ultrasound waves in elastic media*. PhD thesis, Imperial College London, 2008.

[7] H. Froeling. Causes of spurious echoes by ultrasonic wave simulation, 2017.

[8] B. Ghose, K. Balasubramaniam, C.V. Krishnamurthy, and A.S. Rao. Two dimensional fem simulation of ultrasonic wave propagation in isotropic solid media using comsol. In *COMSOL Conference*, 2010.

[9] T. Ihara, N. Tsuzuki, and H. Kikura. Development of the ultrasonic buffer rod for the molten glass measurement. *Progress in Nuclear Energy*, 82:176–183, 2015.

[10] S. Mastromarino. Determination of thermodynamic properties of molten salts, 2017.

[11] MATLAB. *version (R2016a)*. The MathWorks Inc., Natick, Massachusetts, 2016.

[12] S. Mönkölä. Numerical simulation of fluid-structure interaction between acoustic and elastic waves. *Jyväskylä studies in computing; 1456-5390; 133.*, 2011.

[13] NDT. Mode conversion. URL https://www.nde-ed.org/EducationResources/CommunityCollege/Ultrasonics/Physics/modeconversion.htm.

[14] J. Pezant, J.E. Michaels, and T.E. Michaels. An examination of trailing echoes in tapered rods. In *AIP Conference Proceedings*, volume 1096, pages 1627–1634. AIP, 2009.